High-Resolution Reservoir Models Integrating Multiple-Well Production Data

Xian-Huan Wen,* SPE, Stanford U.; **C.V. Deutsch,** SPE, U. of Alberta; and **A.S. Cullick,** Mobil Upstream Strategic Research Center

Summary

This paper presents a method to generate maps of high resolution permeability from multiple well single-phase flow rate and pressure data. The dynamic (i.e., temporal) production data contain important information about the interwell permeability distribution that should be integrated with static data, such as well and seismic data, to generate reservoir models to provide reliable input to reservoir simulation and reservoir management. A two-step procedure is proposed for such data integration: establish the spatial constraints on large-scale permeability trends caused by the production data by means of an inverse technique and construct the detailed geostatistical reservoir models subject to those spatial constraints by means of geostatistical techniques. The single-phase pressure and production data could be provided by permanent pressure gauges, simultaneous multiple well tests, or flow rates under primary depletion.

Production data and reservoir petrophysical properties, specifically permeability, are nonlinearly related through flow equations. Establishing the spatial constraints on permeability resulting from production data calls for the solution of a difficult inverse problem. This paper adapts the sequential self-calibration (SSC) inverse technique to single-phase multiple-well transient pressure and production rate data. The SSC method is an iterative geostatistically based inverse method coupled with an optimization procedure that generates a series of coarse grid two-dimensional (2D) permeability realizations whose numerical flow simulations correctly reproduce the production data. Inverse results with two synthetic data sets show that this SSC implementation is flexible, computationally efficient, and robust.

Fine-scale models generated by downscaling the SSC generated coarse-scale models (by simulated annealing) are shown to preserve the match to the production data at the coarse scale. Finally, reservoir performance prediction results show how the integration of production data can dramatically improve the accuracy of production forecasting with significantly less uncertainty.

Introduction

Optimal reservoir management requires reliable performance forecasts with as little uncertainty as possible. Incomplete data and inability to model the physics of fluid flow at a suitably small scale lead to uncertainty. Uncertainties in the detailed description of reservoir lithofacies, porosity, and permeability are large contributors to uncertainty in reservoir performance forecasting. Reducing this uncertainty can be achieved only by integrating additional data in reservoir modeling.

A large variety of geostatistical techniques have been developed that construct reservoir models conditioned to diverse types of static data, including hard well data and soft seismic data.[1] Commonly, a number of techniques are applied sequentially to model the large reservoir geometry; the lithofacies; and then the petrophysical properties, such as porosity and permeability. However, conventional geostatistical techniques, including Gaussian, indicator, annealing-based, or object-based methods, are not suited to integrate dynamic production data directly.

*Now with Chevron Petroleum Technology Co.

Copyright 1998 Society of Petroleum Engineers

This paper (SPE 52231) was revised for publication from paper SPE 38728, first presented at the 1997 SPE Annual Technical Conference and Exhibition held in San Antonio, Texas, 5–8 October. Original manuscript received for review 21 October 1997. Revised manuscript received 22 June 1998. Revised manuscript approved 3 August 1998.

Production data and reservoir petrophysical properties are related to each other through flow equations, which are highly nonlinear. As a consequence, accounting for dynamic engineering data in geostatistical reservoir modeling is a difficult inverse problem.[2-5] Nevertheless, historical production data are often the most important information because they provide a direct measure of the actual reservoir response to the recovery process that forms the basis for reservoir management decisions. Integrating dynamic production data is an important outstanding problem in reservoir characterization.

Ideally, we want to match all types of production data in the reservoir model at the required resolution directly and simultaneously with other types of geological and geophysical data. A number of inverse techniques have been developed for this purpose.[2,4,6-10] Direct integration at the fine scale is not feasible because the mathematical inversion of the flow equations is computationally intensive, pressure and production data measured at the wells are responding to the spatial variation of larger-scale effective properties, and it is difficult to match production data simultaneously with other static geological and geophysical data. Because of these limitations, currently available inverse techniques are limited to constructing relatively coarse-scale models.

The coarse grid models that could be constructed by direct inversion techniques are usually inadequate for reliable production forecasting. In many practical situations, while keeping models as simple as possible, we would like to create highly resolved models of lithofacies, porosity, and permeability. Our proposal, therefore, is a two-stage approach where we establish the spatial constraints on large-scale permeability trends caused by the production data use of an inverse technique and construct the detailed geostatistical models subject to those spatial constraints and the static data as well.

A review of available inverse techniques has been presented in our previous paper.[11] In this paper, the SSC inverse technique[3,12] is adapted to invert permeability distribution from multiple well, single-phase production data. Under the two-stage approach framework, the SSC method is considered to be an interpretative tool of coding production data into spatial constraints of permeability (i.e., the multiple realizations of coarse grid permeability models) for the first stage (see **Fig. 1**). Then, an annealing-based geostatistical technique is used to construct high resolution reservoir models constrained to the SSC generated coarse grid models for the second stage. The application of the SSC method to synthetic data sets documents the utility and robustness of the method in generating coarse-scale permeability models. The ability to use the coarse grid models to generate fine-scale permeability models that preserve the match of the production data is illustrated. Finally, the importance of integrating production data is illustrated by performing reservoir forecasts on the basis of on the constructed fine-scale reservoir models.

The SSC Method

The available production data include pressure $p_i(t)$ and flow rate $Q_i(t)$ with time t at a number of wells $i = 1, \ldots, n_w$ (n_w = the number of wells). Our goal is to find a set of permeability values for numerical cells in a reservoir model that matches the observed pressure data under the given flow rate and boundary conditions. This match is established by solving the single-phase, slightly compressible flow equation,

$$\nabla\left(\frac{kh}{\mu}\nabla p\right) + Q = hc\phi\frac{\partial p}{\partial t}, \quad \ldots\ldots\ldots\ldots\ldots\ldots\ldots\ldots (1)$$

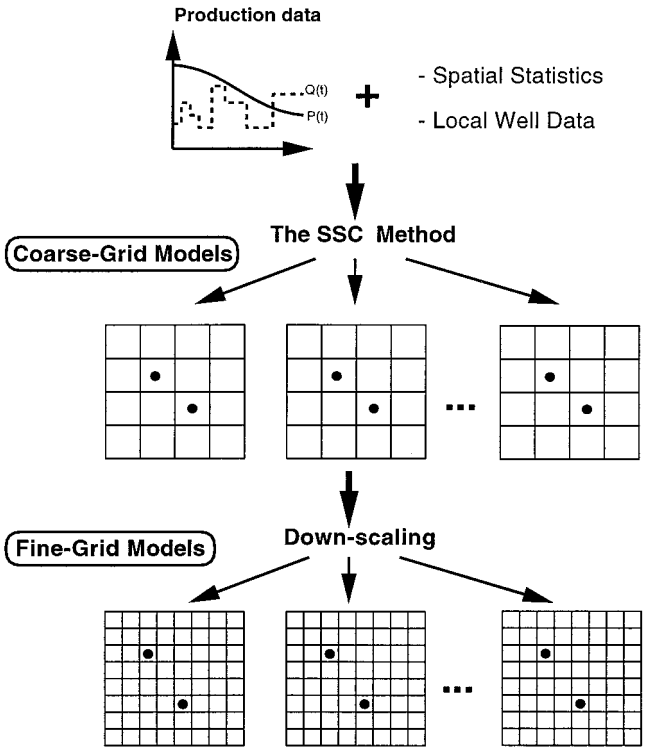

Fig. 1—The SSC method as an interpretative tool for the first stage under the two-stage approach framework. The second stage of constructing fine grid models accounting for the SSC generated coarse grid models is a downscaling problem.

where k = permeability, ϕ = porosity, μ = viscosity, h = the thickness of the reservoir, and c = compressibility. The closeness of the pressure match may be quantified by an objective function,

$$O = \sum_i \sum_t w(i,t)[p_i^{obs}(t) - p_i^{cal}(t)]^2 \quad \ldots\ldots\ldots\ldots\ldots\ldots (2)$$

where $p_i^{obs}(t)$ and $p_i^{cal}(t)$ = observed and numerically calculated pressure data at Well i at time, t, respectively; $w(i, t)$ is the weight assigned to the observed pressure data $p_i(t)$ according to its reliability (accuracy).

The SSC method is an iterative geostatistically based method coupled with an optimization procedure.[3,13] Like geostatistical approaches, the SSC method generates multiple, equally likely realizations of permeability fields honoring different types of available static and dynamic field data. The realizations honor a specified histogram and variogram as modeled from the field data and dynamic pressure data at multiple wells in the sense that the numerical solution of the flow equations in each of the generated realizations matches the measured pressure values at the same well locations.

The unique aspects of the SSC method are the concept of master points and a perturbation mechanism based on kriging. We propose to extend the method for petroleum applications. As an overview, the method can be described as follows (see also **Fig. 2**). First, multiple, initial permeability realizations are created by conventional geostatistical techniques constrained to all static (hard and soft) data and the specified permeability histogram and variogram. Each realization is processed one at a time with the following steps:

1. Solve the flow equations for the current model by use of the specified boundary and production rate conditions. A block-centered finite difference method with a direct matrix solver was used to solve the flow equations in this study. Other numerical methods can also be used for the same purpose.

2. Compare the observed and calculated pressure values at the available wells and at the given time. If the difference is smaller than a preselected tolerance value, this permeability realization is considered to honor the dynamic pressure data, and the procedure stops. Otherwise, proceed to the next step.

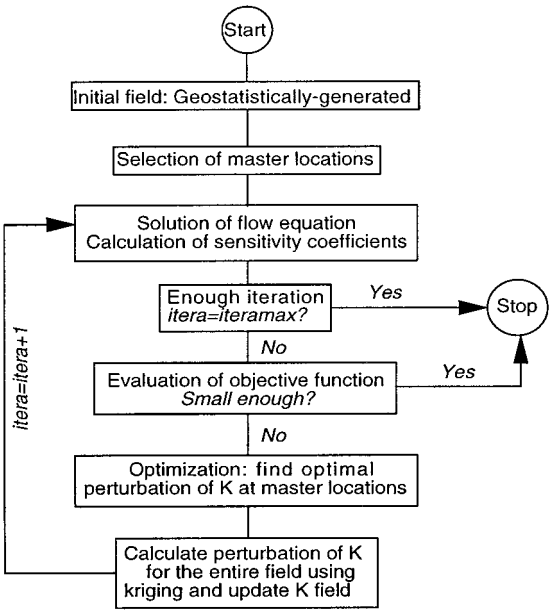

Fig. 2—Flow chart of the SSC method.

3. Select master points and solve an optimization problem to find the optimal perturbations of permeability at the master point locations. The locations of the master points are randomly selected, and the well locations having permeability data are automatically included as master points. The number of master points is about one master point per correlation range of the permeability variogram in each direction. The optimal perturbations minimize the difference between the observed and calculated pressures. The master point concept reduces the space of parameters to be optimized, which significantly improves the computational efficiency of the method.

4. Propagate the perturbation through the entire field by kriging the optimal perturbations determined for the master point locations. The permeability field is updated by adding the smooth perturbation field to the previous permeability field. The variogram used to generate initial models is the same as that used to propagate the permeability perturbations at master points. This would likely preserve the original spatial variation patterns in the permeability field.

5. Loop back to Step 1 until convergence. Typically, fewer than 20 iterations are required.

Sensitivity coefficients (derivatives of pressure with respect to the perturbation of permeability values) at all master point locations at each timestep are needed when solving the optimization problem by a gradient-based method. The efficient calculation of sensitivity coefficients has received significant attention in the literature.[4,8,14,15] Appendix A presents an efficient way to obtain the required sensitivity coefficients as part of the flow solution. Then, a modified gradient projection method is used to obtain the optimal perturbation values at the selected master locations by minimizing the objective function, which is outlined in Appendix B.

It should be noted that the application of the SSC method requires information on the distribution of permeability at the scale of the numerical grid (histogram and variogram). Also, it assumes that the permeability variation in the entire model is governed by a single histogram and a single variogram model, which may limit its application when the permeability variations in a reservoir are caused by the mixture of multiple populations (e.g., controlled by multiple lithofacies or channel objects) or when there are discontinuous features such as faults, channels, or facies boundaries. Furthermore, there is no direct control on the reproduction of the variogram in the updated realizations. Although the variogram models are well reproduced in all of our examples, a posterior check is suggested to ensure that the appropriate inverse results are obtained. Nevertheless, promising results have been obtained in

groundwater hydrology by use of the SSC method with different heterogeneity features, including the identification of nonmulti-Gaussian features and high permeability flow channels.[12,16-18]

Application of the SSC Method

In this section, we use two synthetic examples to evaluate the ability of the SSC method to generate 2D coarse-scale maps of permeability from multiple well production data. In each example, first, a reference permeability model is constructed, and then, the dynamic pressure responses at a number of wells, caused by changing flow rates, are obtained by flow simulation. On the basis of the dynamic flow rate and pressure data and information on the permeability variogram, the SSC method is used to invert for permeability fields that match the production data. Then, the inverted permeability fields are compared with the reference field to evaluate the capability of the SSC method.

Synthetic studies, in which the true permeability model and flow responses are known with precision, make it possible to test the effectiveness and relevance of the technique when only limited data are available by comparing their results with the true reality. Although this information obtained from such tests may be extremely valuable, it is not sufficient to conclude that the method will perform with a similar degree of success when applied to real data.

Also, note that the application of the SSC method assumes that the permeability field is spatially distributed following a single distribution function that can be inferred from field data. A prior model of the variogram must be assumed (or inferred) as well. We will show later that the inversion results are robust to variations in the assumed variogram.

Example 1. The first example is a 2D, 4,000-ft^2 domain that is discretized into 25 × 25 grid cells of 160 × 160 ft. There is a high permeability (500 md) band connecting the lower-left corner and upper-right corner. The permeability in other areas is constant at 10 md (see **Fig. 3**). There are four wells: W1 at the center of the cell (5, 21), W2 at (21, 21), W3 at (5, 5), and W4 at (21, 5). The four boundaries are no-flow boundaries, porosity is assumed to be constant at 0.2, reservoir thickness is 100 ft, viscosity is 0.2 cp, formation compressibility is 10^{-6} psi^{-1}, and well radius is 0.3 ft.

Fig. 4 shows the imposed production rates and the corresponding pressure responses at the different wells solved numerically. The reason for the different shut-in times is to create some well interference so that more information on spatial variations of permeability is contained in the production data. Sensitivity studies, too exhaustive for this paper, were performed with other production scenarios.

On the basis of the production and pressure data at the four wells, the SSC method was used to estimate the spatial distribution of permeability within the domain by use of the same discretization. Initially, a constant permeability with $\ln(k) = 2\ln(\text{md})$ was assumed at all cells, an anisotropic variogram with very long correlation length (8,000 ft) in the 45° direction was assumed to be accessible from other information. The sensitivity of the inverted results to the selection of the anisotropy and initial permeability model will be demonstrated later.

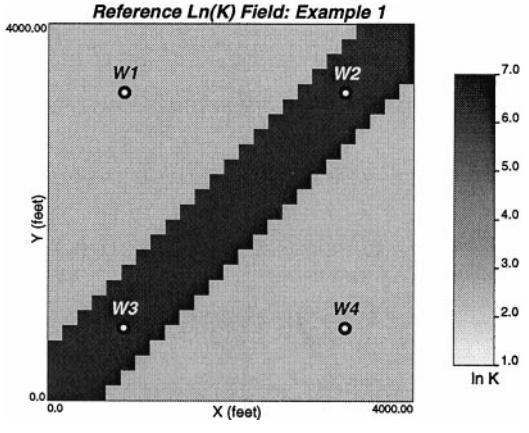

Fig. 3—The reference deterministic permeability field: the first example.

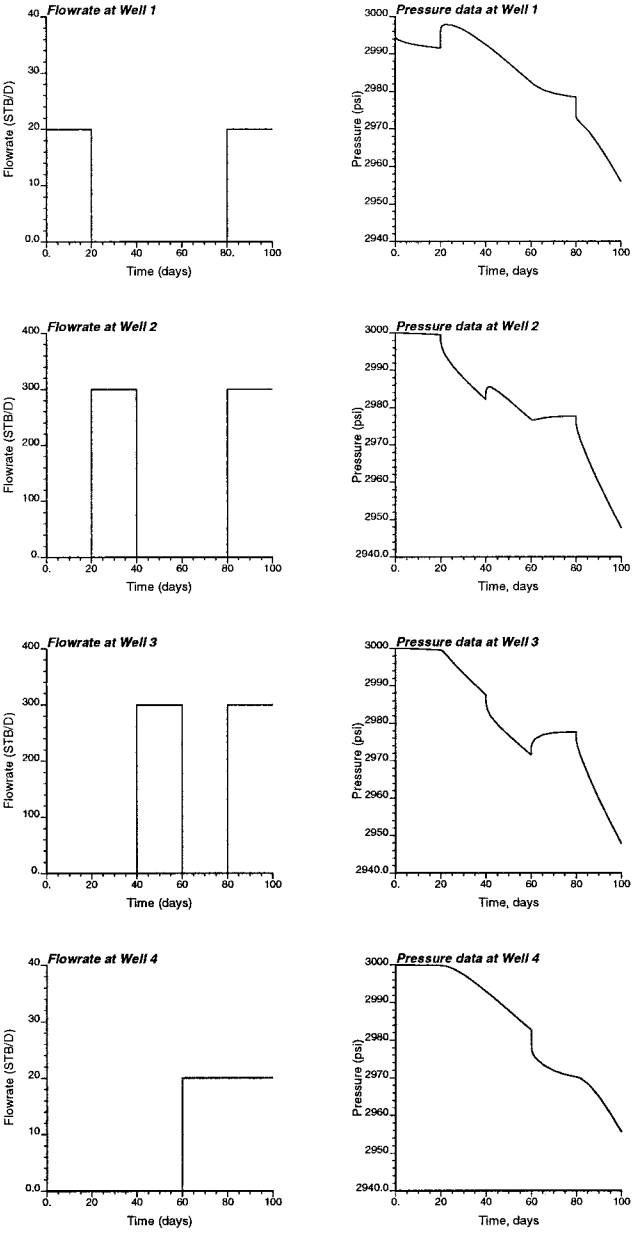

Fig. 4—The production data (left, rates; right, pressures) obtained from the reference field: the first example.

After 20 iterations (5 minutes on an SGI workstation), the pressure responses in the updated permeability field converge to the reference pressure data. **Fig. 5** shows the resulting updated permeability field. The spatially connected high permeability band connecting Wells W2 and W3 is clearly seen. **Fig. 6** shows the pressure values at the four wells computed from the initial uniform permeability field and from the final updated permeability field together with the true results from the reference field. The pressure responses in the initial field deviate dramatically from the true values because of the poor initial model; however, the permeability field updated by the SSC method accurately reproduces the true pressure data at all wells.

Because, in practice, the correct permeability variogram is rarely known, the influence of variogram parameters on inverse results was investigated. Also, the sensitivity of the inverse results to the initial permeability values and the number of master points was studied separately. **Fig. 7** shows the inverse permeability fields by

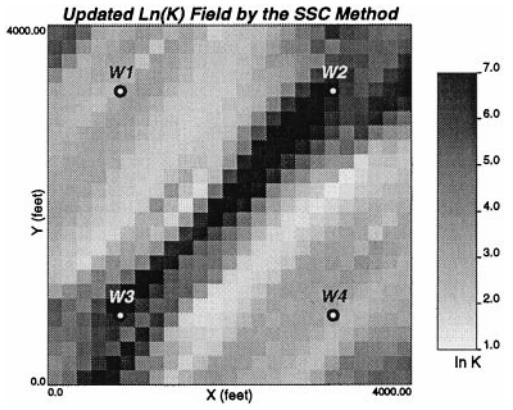

Fig. 5—Final SSC-derived permeability field honoring pressure data from reference permeability field (see Fig. 3).

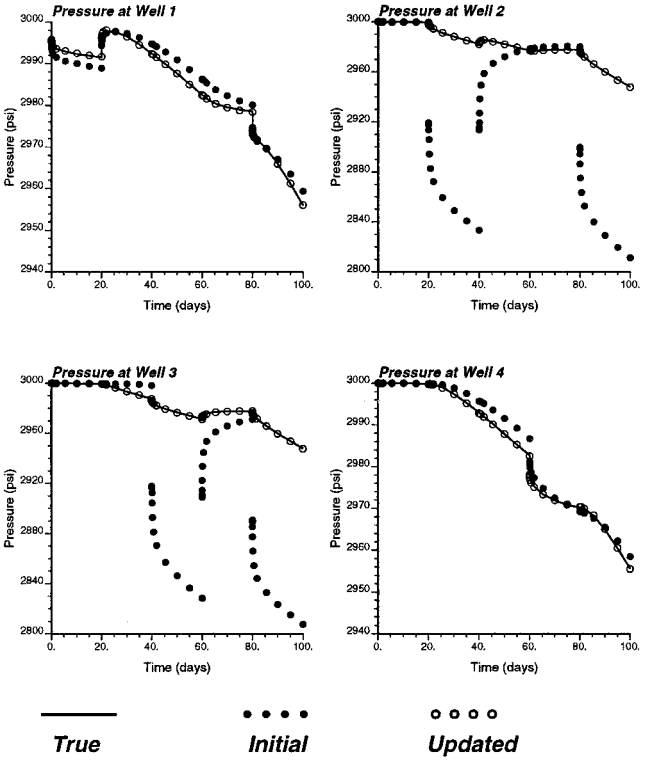

Fig. 6—The pressure responses computed from one typical initial (bullets) and updated (open circles) permeability fields together with the true data (solid lines): the first example.

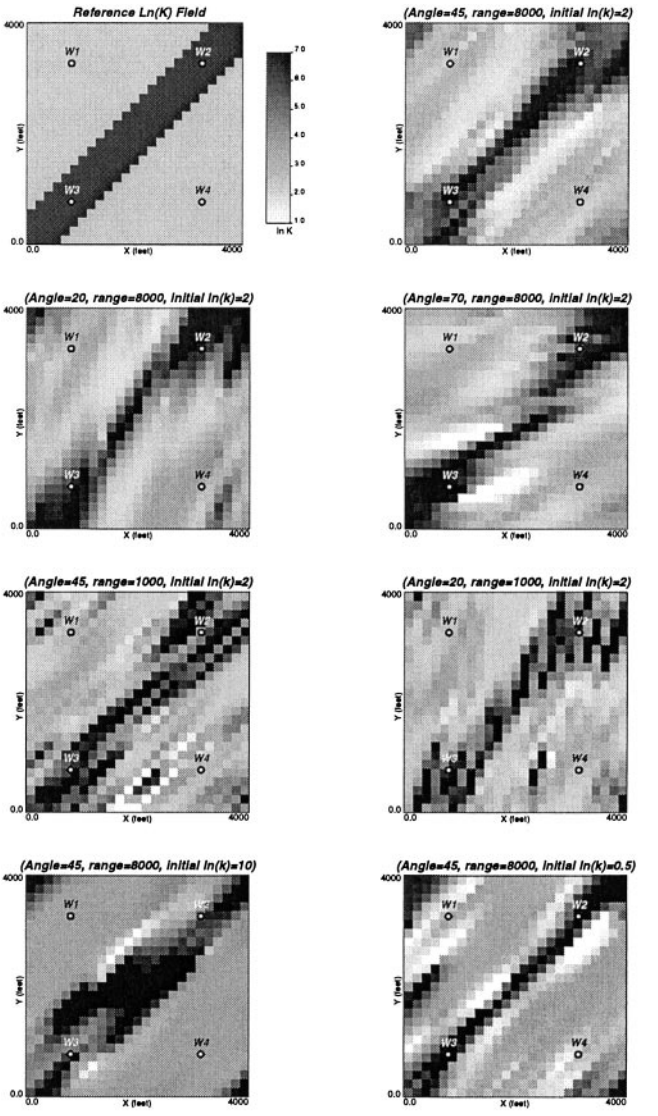

Fig. 7—Inverse permeability fields from the SSC method by use of different variogram parameters and different initial values: the first example.

means of different variogram parameters (correlation range varying from 1,000 to 8,000 ft and principal anisotropy direction varying from 20 to 70°) and different initial permeability values (ranging from $\ln(k) = 0.5$ to 10). In all cases, the high permeability band is always retrieved with good matching of pressure data, indicating the robustness of the SSC method.

Example 2. In the first example, the production data were computed from a coarse grid reference model and the SSC method was used to invert permeability fields on the same coarse grid. This would not usually be the situation in field applications. A more realistic test is to have the synthetic production data generated from simulation by use of a fine grid reference model. Then, the inversion technique is used to create coarse grid models, which are then used as spatial constraints for the construction of high resolution reservoir models (i.e., the two-stage approach, see Fig. 1).

In the second example, a 4,000 × 4,000 ft 2D square domain was discretized into a 100 × 100 fine grid with cell size of 40 × 40 ft. A reference permeability at this fine scale was generated by use of sequential Gaussian simulation (see **Fig. 8**). The mean and variance of $\ln(k)$ were 3.0 and 3.0, respectively. The variogram model used to generate this reference field was anisotropic spherical, with correlation ranges in the two principal directions of 1,700 and 350 ft. The bottom of Fig. 8 shows a coarse grid model (20 × 20) scaled up by geometric averaging from the reference field. This scaled-up coarse grid model is later used for visual comparison with the inverse coarse grid results.

Three wells (W1, W2, and W3) located at the center of the fine-scale cells (58, 88), (13, 43), and (88, 33) produced oil at varying production rates, analogous to the first example. **Fig. 9** shows the corresponding pressure responses. Note that Wells W2 and W3 were connected by relatively high permeabilities, whereas Well W1 was located in a relatively low permeability region. Other parameters used in solving the flow equation for pressure on the fine (100 × 100) were the same as in Example 1.

The SSC method generated coarse grid (20 × 20) permeability realizations for which flow simulation matches the production data. **Fig. 10** shows three initial permeability realizations generated by use of the sequential Gaussian simulation (left) and the corresponding three updated realizations by the SSC method (right). The statistics of the reference coarse grid model (i.e., the bottom of Fig. 8) are used for generating these realizations [i.e., mean and variance of $\ln(\bar{k}_v)$ are 3.0 and 2.03, respectively; correlation lengths are 1,800 and 400 ft in X and Y directions, respectively]. We can see

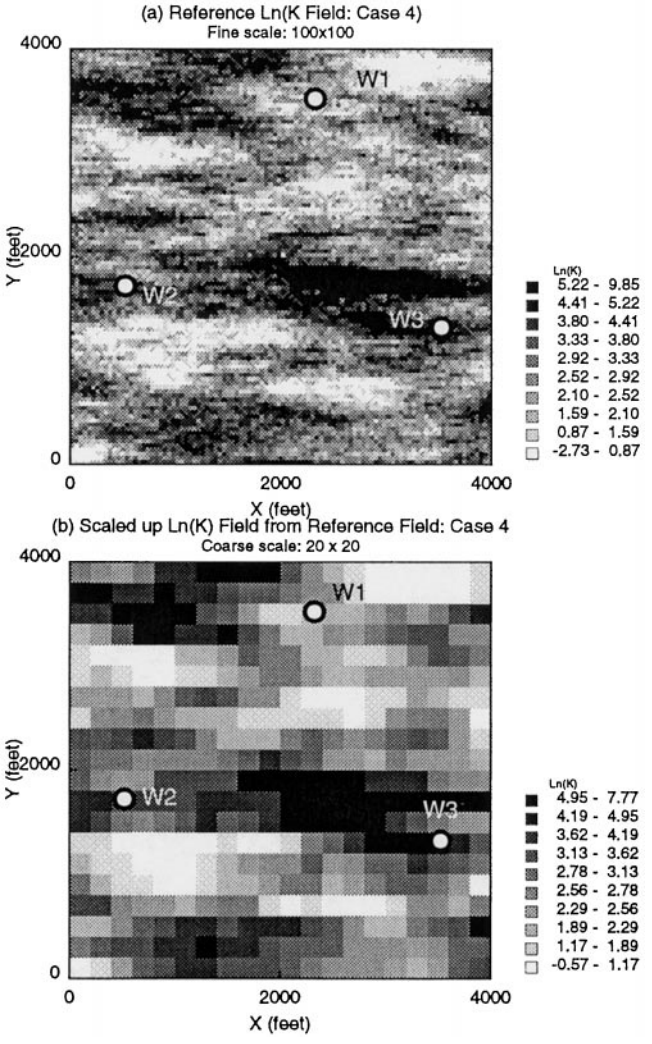

Fig. 8—(a) The reference permeability field at fine scale. (b) The scaled up coarse grid permeability model: the second example.

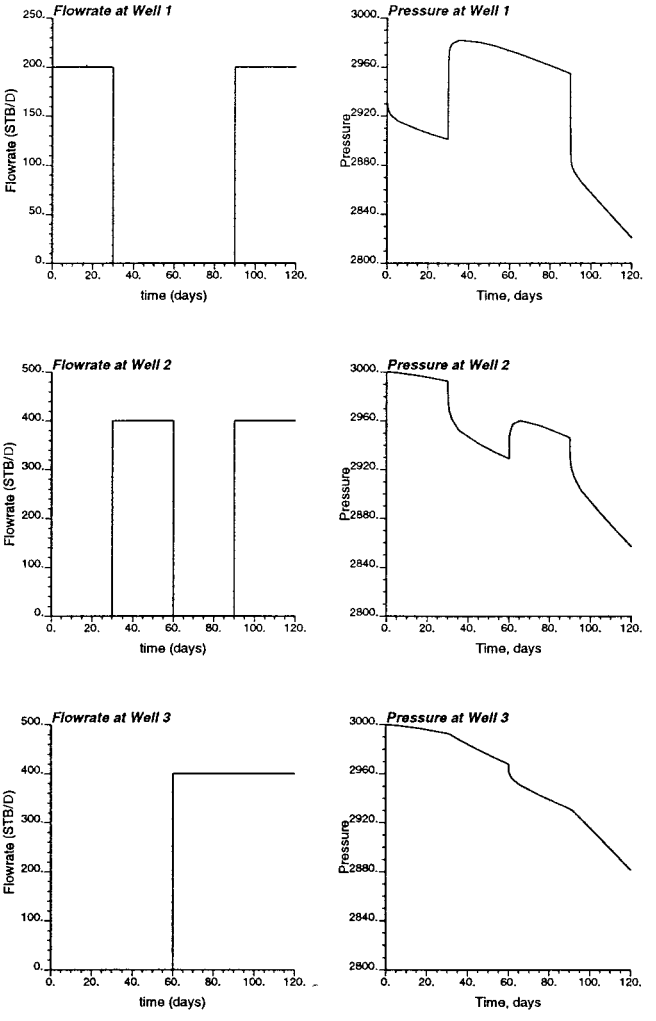

Fig. 9—The production data (left, rates; right, pressures) obtained from the reference field at fine scale: the second example.

the large differences among the initial realizations, all of which deviate significantly from the reference coarse grid model (shown at the bottom of the figure). However, the spatial variation patterns in the updated realizations are much closer to the reference field, yet the difference from realization to realization is much smaller compared with the initial realizations. **Fig. 11** shows the pressure responses computed from a typical initial realization and its corresponding updated permeability realization compared with the true pressure data. The true pressure response is reproduced with high accuracy by the updated field, whereas the initial field's pressure responses deviate significantly from the true data.

We generated 300 coarse grid $\ln(\bar{k}_v)$ realizations by use of the SSC method, from which the ensemble mean and standard deviation fields were computed and compared with the 300 initial fields (**Fig. 12**). **Fig. 13** shows the histograms of coarse grid permeability values at two selected locations, A and B, (see Fig. 12) from the 300 initial and updated realizations. Fig. 12 shows the reduced standard deviation (i.e., uncertainty) from the updated fields, particularly in the areas around the wells. Even away from the wells, the updated fields have lower standard deviations (e.g., Locations A and B in Fig. 13).

Construction of Fine-Scale Permeability Models

With the SSC method, a series of equally likely realizations of coarse grid permeability fields can be generated, all of which share the same histogram, variogram, and production data. Usually, more detailed geostatistical models are required for flow simulation predictions of reservoir performance. In this section, we demonstrate the promise of the two-stage approach to integrate production data, with the SSC results as the first stage. Constructing fine-scale models that honor the coarse grid realizations is a problem of downscaling.

Simulated annealing is one method that can construct fine-scale permeability models based on the coarse grid realizations as well as honor information on the histogram and variogram of fine-scale permeability.[19] Our first approach was to use annealing by adding an additional component to the objective function to represent the difference between the coarse grid permeability values and the power averages of fine-scale permeabilities within the same coarse block, i.e.,

$$O_{mw} = \sum_{i=1}^{n_{\text{coarse grid}}} [\bar{k}_v(\mathbf{u}_i) - \bar{k}_v^*(\mathbf{u}_i)]^2, \quad \ldots\ldots\ldots\ldots\ldots\ldots (3)$$

where $n_{\text{coarse grid}}$ = the number of blocks on coarse grid model, $\bar{k}_v(\mathbf{u}_i)$ = the inverse permeability value at coarse block $\mathbf{u}_i$, and $\bar{k}_v^*(\mathbf{u}_i)$ = the ω power average of fine grid permeability values within the coarse block $\mathbf{u}_i$, which is given as

$$\bar{k}_v^*(\mathbf{u}_i) = \left[\frac{1}{N}\sum_{\mathbf{u}_i \in V} k(\mathbf{u}_i)^{\omega}\right]^{1/\omega}, \quad \ldots\ldots\ldots\ldots\ldots\ldots (4)$$

where N = the number of fine grid cells within a coarse block V. Different fine grid permeability models can be constructed, each of which matches the corresponding coarse grid permeability realization. The value of ω should be calibrated from the corresponding upscaling procedure, which is out of the scope of this study.

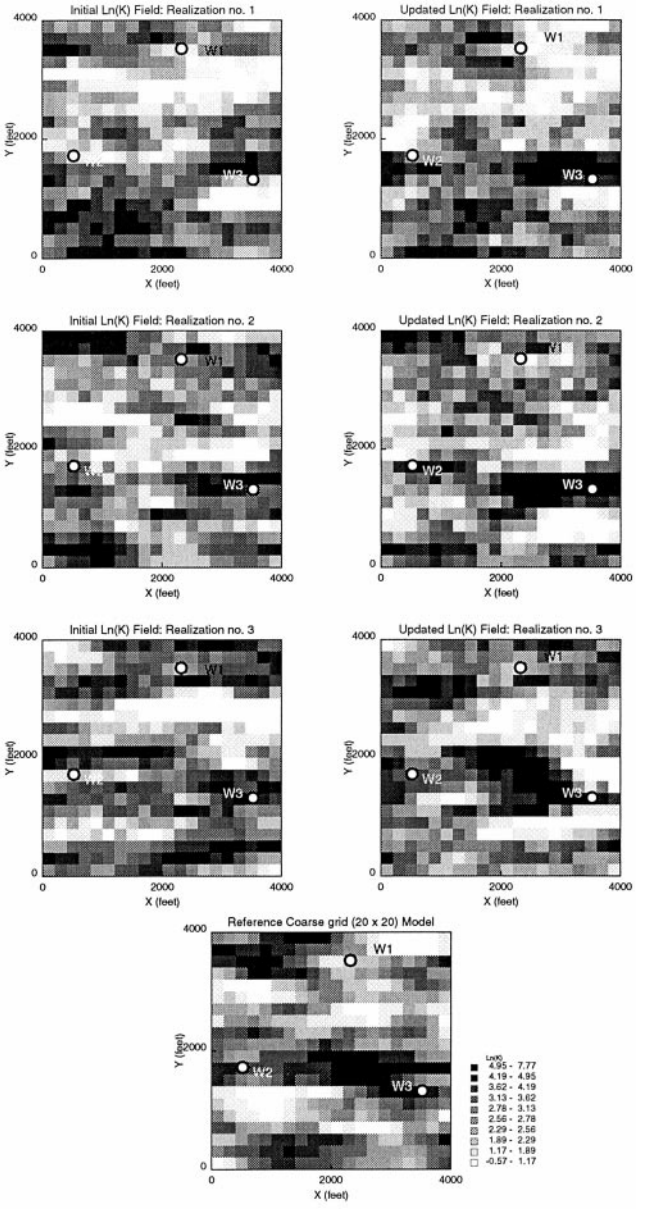

Fig. 10—Three initial permeability realizations (left) and the corresponding updated fields (right) from the SSC method.

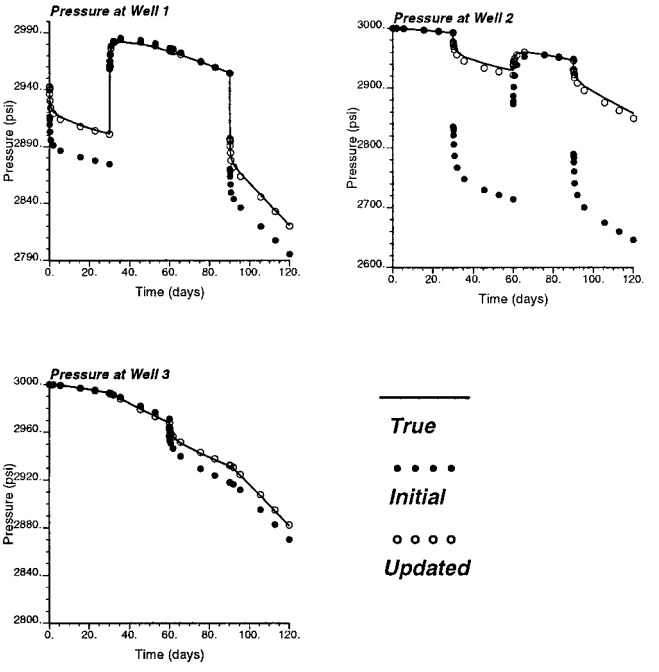

Fig. 11—The pressure responses computed from the typical initial and updated permeability fields together with the true data in a typical realization: the second example.

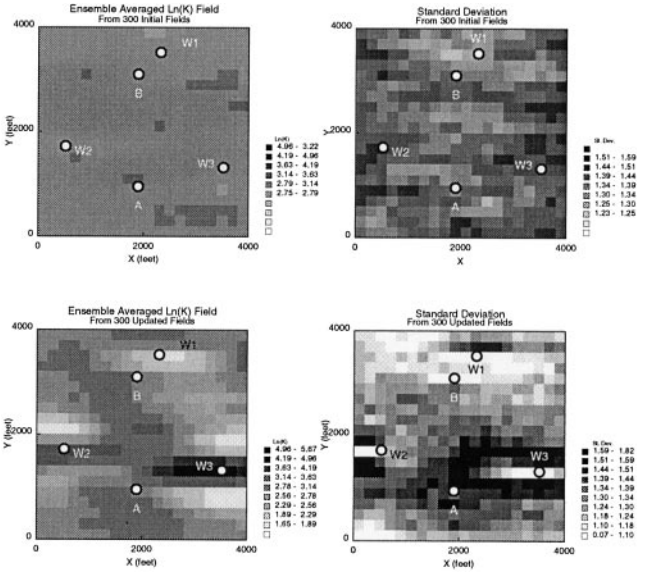

Fig. 12—The ensemble averaged permeability field (left) and the corresponding standard deviations (right) from 300 initial (top) and updated (bottom) realizations: the second example.

Fig. 14 shows two realizations of fine grid (100 × 100) permeability generated by this annealing technique and compared with the corresponding coarse grid (20 × 20) images from the SSC inversion in the second example. The objective function in the annealing process includes histogram, variogram, and coarse grid permeability (i.e., Eq. 3). The histogram and variogram used to construct the fine grid models were taken from the fine grid reference model and geometric averaging ($\omega \rightarrow 0$) was used. Other types of data (e.g., seismic data) could also be honored at this stage.

To check whether the fine grid permeability models still reproduce the dynamic production data, the pressure responses at the wells were solved on the two fine grid models shown in Fig. 14. **Fig. 15** shows the results (open circles) compared with the true responses from the reference field (solid lines) and the responses from the coarse grid model (bullets). The pressure responses are closely reproduced in the annealing-based fine grid permeability models. This indicates the promise of the two-stage geological coding approach to integrate production data.

An alternative and more sophisticated approach for constructing fine grid models by use of the coarse grid spatial representations is to compute local conditional distributions of coarse grid permeability at each coarse gridblock as given in Fig. 13, then use simulated annealing or other geostatistical methods to construct fine grid models integrating these probability constraints of the coarse grid values.[20] Nevertheless, the simpler approach presented earlier may see more extensive use in practice.

Improvement of Performance Prediction From Production Data Integration

Finally, we demonstrate the importance of integrating production data by predicting the reservoir performance in Example 2 by use of two sets of fine-scale (100 × 100) geostatistical models: one generated by the sequential Gaussian simulation not accounting for the production data and the other generated by simulated annealing accounting for the coarse-scale spatial representations derived from the production data as discussed previously. On the right of Fig. 14 two realizations of the second model are shown. The reservoir was

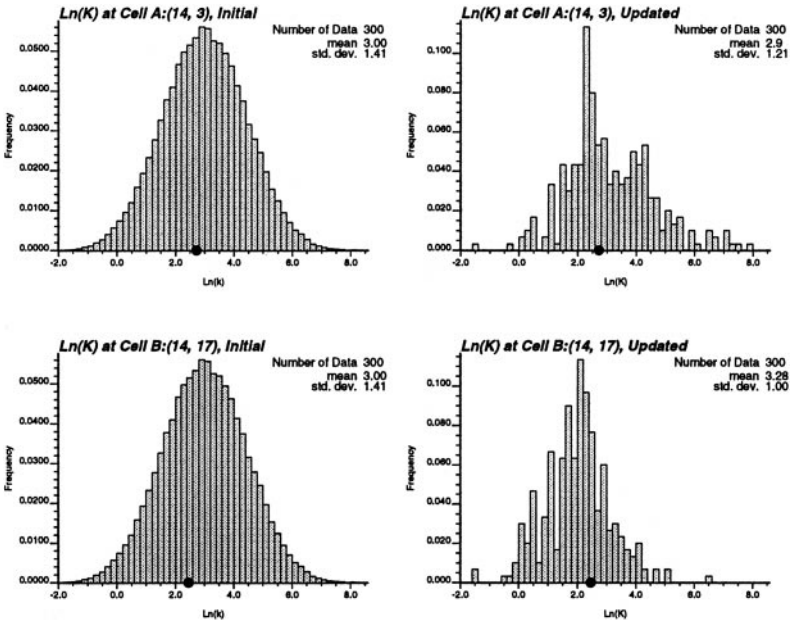

Fig. 13—The histograms of coarse grid permeability values at Locations A and B (see Fig. 12) computed from 300 initial (left) and updated (right) realizations: the second example. The bullets are the values from the reference coarse field at the same locations.

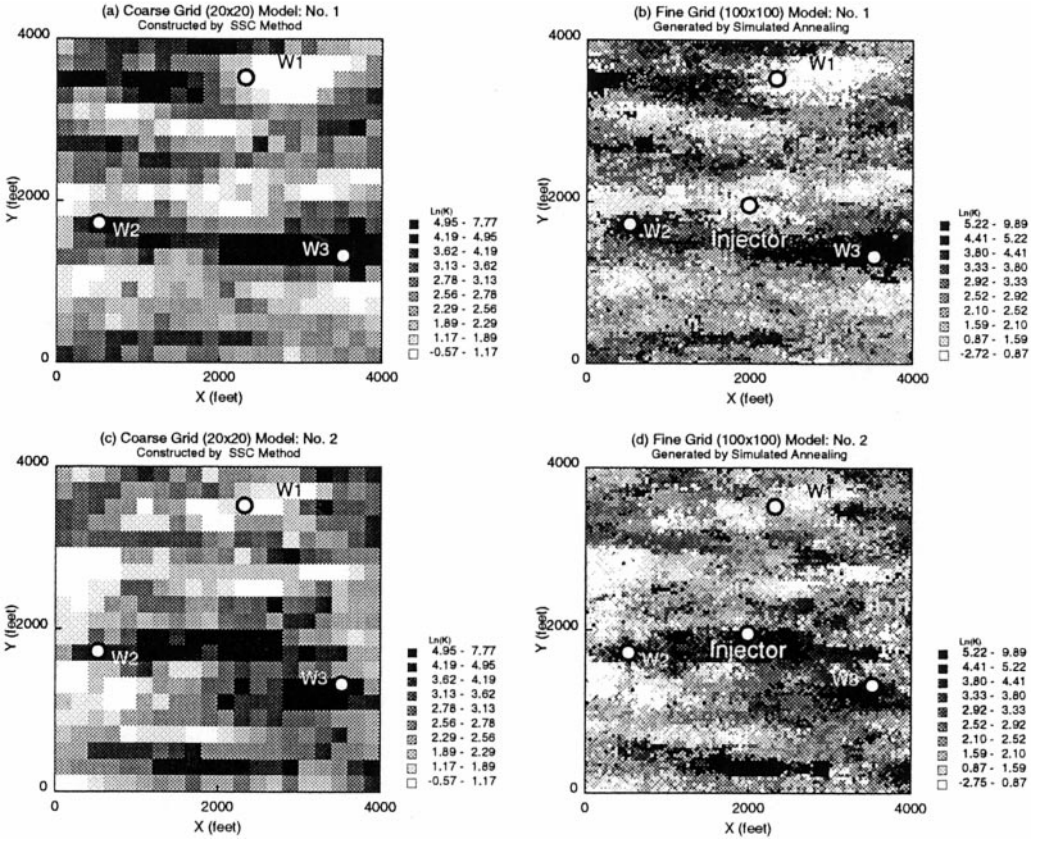

Fig. 14—Two realizations of fine grid models (right), constructed by the simulated annealing method, that honor the coarse grid models generated by the SSC method (left).

under single-phase production before 120 days. The pressure data of the 120-day production were matched in the second model. At 120 days, a water injection well located at the center of Cell (50, 49) began injecting water at a constant rate of 20,000 B/D (see Fig. 14). The three wells (W1, W2, and W3) were producing with constant pressure of 1,000 psi.

Figs. 16 and 17 show the comparisons of predicted total produced oil and water cuts in three wells (W1, W2, and W3) from 30 realizations of both models, respectively. The true results computed from the reference fine-scale model are plotted as the thick, light curves. It is evident that the reservoir models not conditioned to the production data overpredict oil production rates, severely overpre-

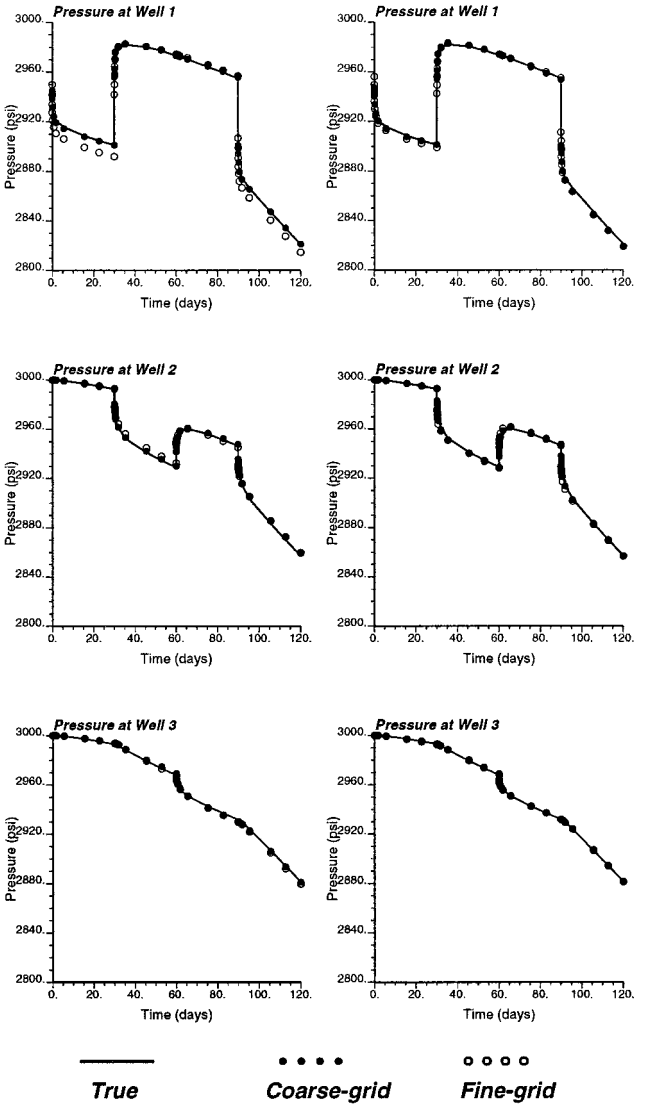

Fig. 15—The comparison of pressure responses computed from the two fine and coarse grid models shown in Fig. 14 to the true results.

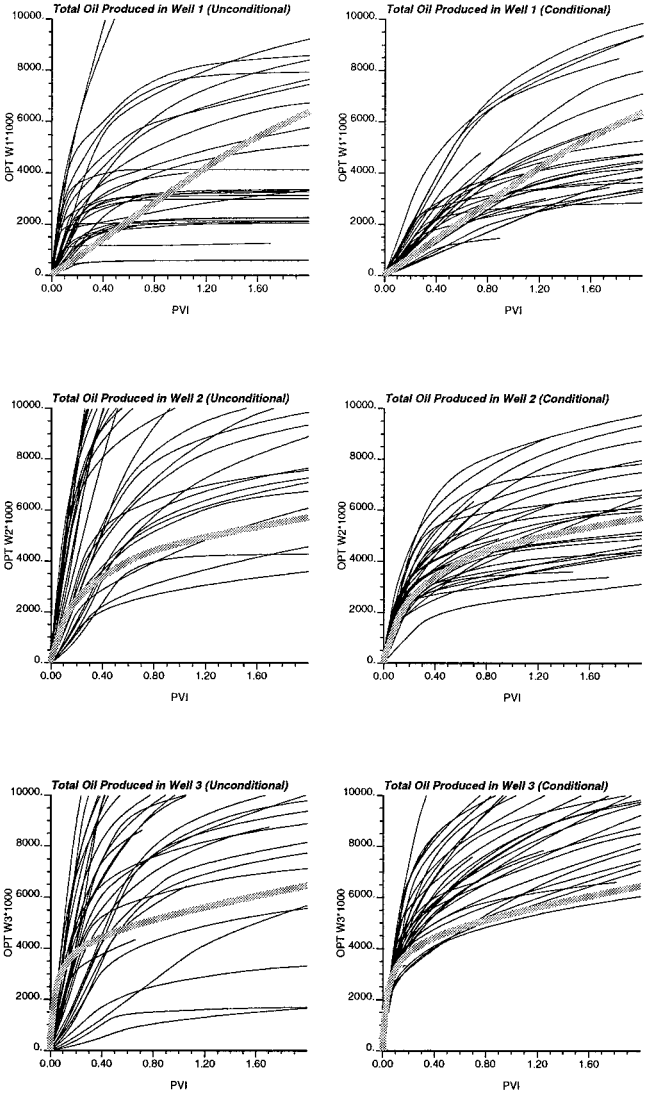

Fig. 16—The total oil production rates at the producing wells from 30 unconditioned (left) and conditioned (right) realizations. The thick light curves are results from the reference true field.

dict water cuts at W1, and underpredict water cuts at W2 and W3 with large uncertainty. When the production data are integrated, the predicted performance is much closer to the true results with significantly less uncertainty. The low permeability barrier in the reference fine grid model between the injection well and W1 is not well captured in the inverse coarse grid models. Also, the variogram distance between the injection well and W1 is larger than other well pairs, so there are more permeability variations between these two wells. These may explain why the predictions are so far from the true results in W1 compared with the results at W2 and W3.

Fig. 18 shows the histograms of total oil production rates of the entire field (the top row) as well as the water cuts at individual wells (the bottom three rows) from 200 unconditioned and conditioned models when the injected water is at pore volume injected (PVI) of 1.0. The true values from the reference field are shown in the same figure by bullets. It is clearly shown that integrating production data shows significant improvement in forecasting results in terms of accuracy and uncertainty.

Conclusions

The SSC method appears to be flexible and computationally efficient for integrating single-phase multiple well pressure/rate data. It is well suited as an interpretive tool for extracting spatial representations (i.e., 2D coarse grid models) from production data for the two-stage approach. Results from the synthetic examples further indicate that the two-stage approach has promise to integrate production data. Reservoir performance predictions show that the integration of production data can dramatically improve accuracy and reduce uncertainty of reservoir simulation predictions for reservoir management.

Extensive work is required to explore the limits of the SSC method and to establish the practical range of application. Ongoing research will investigate the integration of multiple-phase production data and extensions of these methods to coarse-scale models with different lithofacies and to three-dimensional models. A method of analyzing the degree of interference of production data from different wells may also be useful to guide the selection of production data used in the inversion to increase the computational efficiency.

Nomenclature

$[A]$ = transmissibility matrix
$[B]$ = right hand side of discretized flow equation
c = formation compressibility, psi^{-1}
h = thickness of reservoir, ft
k = permeability, md
$\bar{k}_v$ = coarse grid permeability from inversion, md
$\bar{k}_v^*$ = power average of fine grid permeability, md

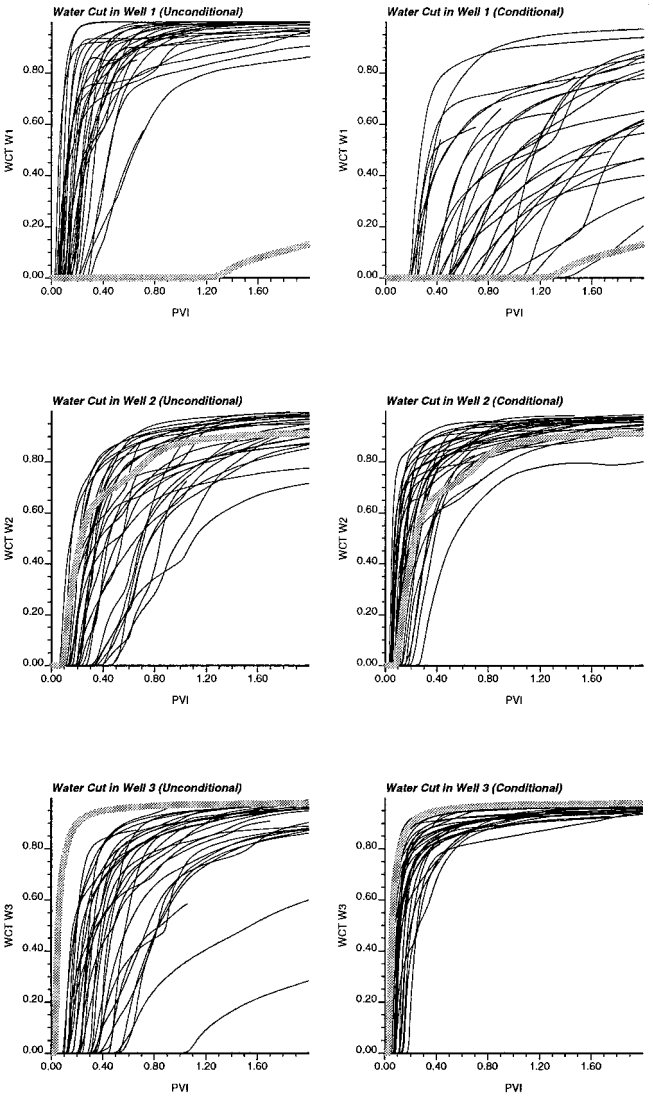

Fig. 17—The water cuts at the producing wells from 30 unconditioned (left) and conditioned (right) realizations. The thick light curves are results from the reference true field.

k_{krig} = kriging estimation of permeability, md
n_m = number of master points
n_t = number of timesteps
n_w = number of wells
N = number of fine grid cells in a coarse block
O = objective function
p = pressure, psi
Q = production rate, B/D
$\{S\}$ = sensitivity coefficient vector
t = time, days
V = volume of coarse gridblock
$[W]$ = inverse covariance of observation errors
α = amplitude factor for constraint interval
β = moving step in updating parameters
Δk = permeability perturbation, md
μ = viscosity, cp
σ_{krig} = standard deviation of kriging estimation
ϕ = porosity
ω = averaging power

Superscript

cal = calculated
obs = observed

Acknowledgments

We thank Mobil Oil Corp. for permission to present this work. Technical support from and discussions with J.R. Capilla and J.J. Gómez-Hernández at Polytechnic U. of Valencia, Valencia, Spain, on the use of SSC method are greatly acknowledged.

References

1. Deutsch, C.V., and Journel, A.G.: *GSLIB: Geostatistical Software Library and User's Guide*, Oxford U. Press, New York City (1992).
2. Feitosa, G.S., *et al.*: "Determination of Reservoir Permeability Distributions From Well Test Pressure Data," *JPT* (1994) **46,** No. 7, 607.
3. Gómez-Hernández, J.J., Sahuquillo, A., and Capilla, J.E.: "Stochastic Simulation of Transmissivity Fields Conditional to Both Transmissivity and Piezometric Data. 1. The Theory, *J. Hydrology* (1998) **203,** 162.
4. Landa, J.L., *et al.*: "Reservoir Characterization Constrained to Well-Test Data: A Field Example," paper SPE 36511 presented at the 1996 SPE Annual Technical Conference and Exhibition, Denver, Colorado, 6–9 October.
5. Tarantola, A.: *Inverse Problem Theory: Methods for Data Fitting and Model Parameter Estimation*, Elsevier, Amsterdam, The Netherlands (1987).
6. Chu, L., Komara, M., and Schatzinger, R.A.: "An Efficient Technique for Inversion of Reservoir Properties Using Iteration Method," paper SPE 36512 presented at the 1996 SPE Annual Technical Conference and Exhibition, Denver, Colorado, 6–9 October.
7. He, N., Reynolds, A.C., and Oliver, D.S.: "Three-Dimensional Reservoir Description From Multiwell Pressure Data and Prior Information," paper SPE 36509 presented at the 1996 SPE Annual Technical Conference and Exhibition, Denver, Colorado, 6–9 October.
8. Oliver, D.S.: "Incorporation of Transient Pressure Data Into Reservoir Characterization," *In Situ* (1994) **18,** No. 3, 243.
9. Reynolds, A.C., Chu, L., and Oliver, D.S.: "Reparameterization Techniques for Generating Reservoir Descriptions Conditioned to Variograms and Well-Test Pressure," paper SPE 30588 presented at the 1995 SPE Annual Technical Conference and Exhibition, Dallas, 22–25 October.
10. Vasco, D.W., Datta-Gupta, A., and Long, J.C.S.: "Integrating Field Production History in Stochastic Reservoir Characterization," paper SPE 36568 presented at the 1996 SPE Annual Technical Conference and Exhibition, Denver, Colorado, 6–9 October.
11. Wen, X.H., Deutsch, C.V., and Cullick, A.S.: "A Review of Current Approaches to Integrate Flow Production Data in Geological Modeling," report 10, Stanford Center for Reservoir Forecasting, Stanford, California (May 1997).
12. Wen, X.H.: "Stochastic Simulation of Groundwater Flow and Mass Transport in Heterogeneous Aquifers: Conditioning and Problem of Scales." PhD dissertation, Polytechnic U. of Valencia, Valencia, Spain (1996).
13. Capilla, J.E., Gómez-Hernández, J.J., and Sahuquillo, A.: "Stochastic Simulation of Transmissivity Fields Conditioning to Both Transmissivity and Piezometric Data. 2. Demonstration in a Synthetic Case," *J. Hydrology* (1998) **203,** 175.
14. Chu, L., Reynolds, A.C., and Oliver, D.S.: "Computation of Sensitivity Coefficients for Conditioning the Permeability Field to Well-Test Pressure Data," *In Situ* (1995) **19,** No. 2, 179.
15. Datta-Gupta, A., Vasco, D.W., and Long, J.C.S.: "Sensitivity and Spatial Resolution of Transient Pressure and Tracer Data for Heterogeneity Characterization," paper SPE 30589 presented at the 1995 SPE Annual Technical Conference and Exhibition, Dallas, 22–25 October.
16. Wen, X.H.: "Geostatistical Methods for Prediction of Mass Transport in Groundwater," PhD dissertation, Royal Inst. of Technology, Stockholm, Sweden (1995).
17. Wen, X.H., *et al.*: "The Significance of Conditioning on Piezometric Head Data for Predictions of Mass Transport in Groundwater Modeling," *Mathematics in Geology* (October 1996) **28,** No. 7, 961.
18. Zimmerman, D.A. *et al.*: "Some Results From a Comparison Study of Geostatistically-Based Inverse Techniques," Sandia Natl. Laboratories, Albuquerque, New Mexico (1995).
19. Deutsch, C.V.: "Annealing Techniques Applied to Reservoir Modeling and the Integration of Geological and Engineering (Well Test) Data," PhD dissertation, Stanford U., Stanford, California (1992).

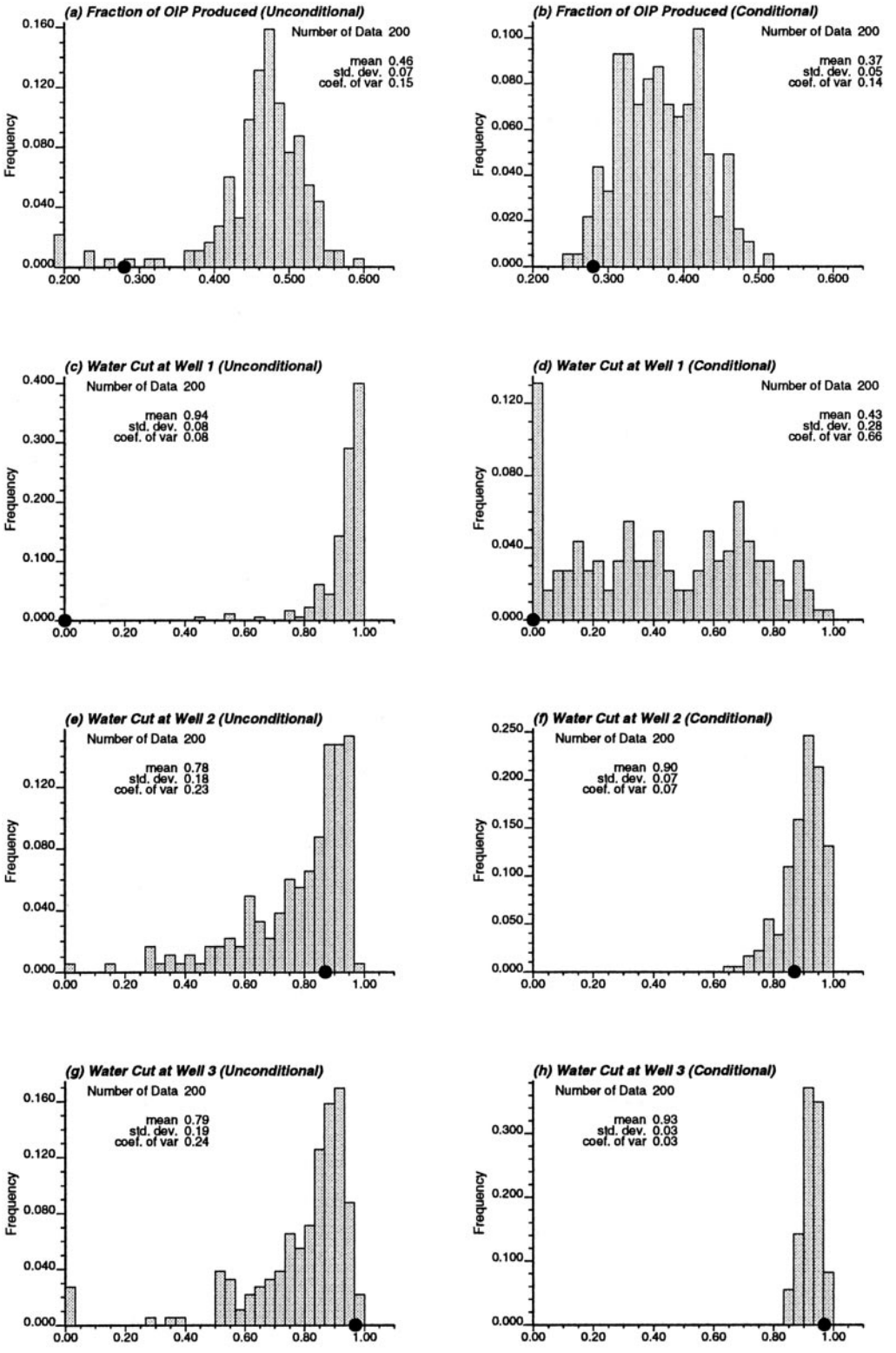

Fig. 18—The histograms of total oil produced (top row) and water cuts at three wells (bottom 3 rows) from 200 unconditioned (left) and conditioned (right) realizations when the injected water is at pore volume injected of 1.0. Bullets are the true results from the reference field.

20. Deutsch, C.V., and Wen, X.H.: "Integrating Large-Scale Soft Data by Simulated Annealing and Probability Constraints," report 10, Stanford Center for Reservoir Forecasting, Stanford, California (May 1997).

Appendix A—Calculation of Sensitivity Coefficients

Discretization of the Flow Eq. 1, with an implicit scheme leads to the matrix notation

$$[A]\{p\}^{t+1} = [B]\{p\}^{t} + \{f\}^{t}, \quad \ldots\ldots\ldots\ldots\ldots\ldots\ldots\ldots \text{(A-1)}$$

where $[A]$ = the transmissibility matrix that accounts for spatial and time discretizations, as well as boundary conditions, $[B] = [hc\phi]/\Delta t_{t+1}$, and $\{f\}^{t}$ = the right hand side matrix that accounts for the load vector (production or injection) and flow boundary conditions. The solution of pressure at time $t + 1$ is obtained by inverting matrix $[A]$, that is,

$$\{p\}^{t+1} = [A]^{-1}[B]\{p\}^{t} + [A]^{-1}\{f\}^{t}. \quad \ldots\ldots\ldots\ldots\ldots\ldots\ldots \text{(A-2)}$$

The sensitivity coefficients at timestep $t + 1$ can be calculated right after the pressure at time $t + 1$ is obtained. The perturbation of parameter k_m can be written as

$$[A]\frac{\partial\{p\}^{t+1}}{\partial\Delta k_m} + \frac{\partial[A]}{\partial\Delta k_m}\{P\}^{t+1} = \frac{\partial[B]}{\partial\Delta k_m}\{p\}^t + [B]\frac{\partial\{p\}^t}{\partial\Delta k_m} + \frac{\partial\{f\}^t}{\partial\Delta k_m}, \quad m = 1, \ldots, n_m, \quad \text{(A-3)}$$

where n_m = total number of master points, thus,

$$\frac{\partial\{P\}^{t+1}}{\partial\Delta k_m} = \frac{\partial[B]}{\partial\Delta k_m}\{p\}^t + [B]\frac{\partial\{p\}^t}{\partial\Delta k_m} + \frac{\partial\{f\}^t}{\partial\Delta k_m} - \frac{\partial[A]}{\partial\Delta k_m}\{p\}^{t+1}, \quad m = 1, \ldots, n_m. \quad \text{(A-4)}$$

Note that Eq. A-4 has the same form as Eq. A-1 and matrix $[A]$ has just been inverted when solving for the pressure $\{p\}^{t+1}$. The sensitivity coefficients can be obtained at the same timestep, $t + 1$, by simple matrix operations, that is,

$$s_{m,t+1} = \frac{\partial\{p\}^{t+1}}{\partial\Delta k_m} = [A]^{-1}[B]\frac{\partial\{p\}^t}{\partial\Delta k_m} + [A]^{-1}\frac{\partial[B]}{\partial\Delta k_m}\{p\}^t + [A]^{-1}\frac{\partial\{f\}^t}{\partial\Delta k_m} - [A]^{-1}\frac{\partial[A]}{\partial\Delta k_m}\{P\}^{t+1}, \quad m = 1, \ldots, n_m. \quad \text{(A-5)}$$

The elements of matrices $\partial[A]/\partial\Delta k_m$, $\partial[B]/\partial\Delta k_m$, and $\partial\{f\}^t/\partial\Delta k_m$ can be directly computed from the expressions of elements in matrices $[A]$, $[B]$, and $\{f\}$. $\partial\{P\}^0/\partial\Delta k_m = 0$.

The efficient calculation of sensitivity coefficients has received significant attention in the literature.[4, 8, 14, 15]

Appendix B—Minimization of Objective Function

The objective function given in Eq. 2 can be written in the matrix form

$$O(\{p^{cal}\}) = \sum_{t=1}^{n_t}(\{p^{cal}\}_t - \{p^{obs}\}_t)^T[W]_t(\{p^{cal}\}_t - \{p^{obs}\}_t), \quad \text{(B-1)}$$

where $\{p^{cal}\}_t = \{p^{cal}_{t,1}, p^{cal}_{t,2}, \ldots, p^{cal}_{t,n_w}\}$ and $\{p^{obs}\}_t = \{p^{obs}_{t,1}, p^{obs}_{t,2}, \ldots, p^{obs}_{t,n_w}\}$ are the numerically calculated and observed pressures at Well $i = 1, \ldots, n_w$ and time $t = t_1, \ldots, t_n$. $[W]_t$ is the inverse covariance matrix of observation errors at time t. If pressure measurement errors at different wells are independent, $[W]_t$ is a diagonal matrix with the form

$$[W]_t = \begin{bmatrix} w_{1,t} & & & \\ & w_{2,t} & & \\ & & \ldots & \\ & & & w_{n_w,t} \end{bmatrix}. \quad \text{(B-2)}$$

Objective function (Eq. B-1) is a nonlinear function of the model parameters we need to compute (i.e., the perturbations of permeability at master locations, $\{M\} = \{\Delta k_1, \Delta k_2, \ldots, \Delta k_{n_m}\}$). We linearize the objective function by approximating the pressure data by retaining its first order Taylor expansion, i.e.,

$$\{p^{cal}\}^1_t \approx \{p^{cal}\}^0_t + \frac{\partial\{p\}_t}{\partial\{M\}}\{M\}, \quad \text{(B-3)}$$

where $\{S\}_t = \partial\{p\}_t/\partial\{M\} = \{s_{1,t}, s_{2,t}, \ldots, s_{n_m,t}\}$ is the sensitivity vector at time t with respect to the permeability perturbation at Location m computed as presented in Appendix A, with $s_{m,t} = \partial\{p\}_t/\partial\{\Delta k_m\}$. $\{p^{cal}\}^0_t$ and $\{p^{cal}\}^1_t$ are pressure values at time t before and after introducing a perturbation matrix $\{M\}$. With this linear approximation, after some manipulation, we can write our objective function (Eq. B-1) as

$$O(\{p^{cal}\}^1) = O(\{p^{cal}\}^0) + \sum_{t=1}^{n_t}\{D\}^T_t\{M\} + \sum_{t=1}^{n_t}\{M\}^T[C]_t\{M\}, \quad \text{(B-4)}$$

where the elements of matrices $\{D\}_t$ and $\{C\}_t$ are expressed as

$$d_{k,t} = 2(\{p^{cal}\}_t - \{p^{obs}\}_t)^T[W]_t\{S\}_t \quad \text{(B-5)}$$

and

$$c_{k_1k_2,t} = (\{S\}_t)^T[W]_t\{S\}_t. \quad \text{(B-6)}$$

The constraints used for minimizing the objective function (Eq. B-4) are simply the possible minimum and maximum values of perturbations, i.e.,

$$\{\Delta k_{\min}\} \leqq \{M\} \leqq \{\Delta k_{\max}\} \quad \text{(B-7)}$$

that is

$$[I]\{M\} \leqq \{\Delta k_{\max}\} \quad \text{(B-8)}$$

and

$$-[I]\{M\} \leqq \{\Delta k_{\min}\}, \quad \text{(B-9)}$$

where $[I]$ = an $n_m \times n_m$ identity matrix, $\{\Delta k_{\min}\} = \min\{k^0, k_{krig} - \alpha\sigma_{krig}\}$ and $\{\sigma k_{\max}\} = \max\{k^0, k_{krig} + \alpha\sigma_{krig}\}$. $\{k^0\}$ = the vector of permeability values at master points in the initial field, $\{k_{krig}\}$ and $\{\sigma_{krig}\}$ = kriging estimations and the corresponding kriging standard deviations, respectively, at the master points, based on available measured permeability data. If there are no prior k measurements, $\{k_{krig}\}$ and $\{\sigma_{krig}\}$ can be selected as the mean and standard deviation of the desired permeability histogram. α = a constant value that specifies the interval size of the constraints.

This formulation is a standard quadratic optimization problem. In the current SSC code, we solve this optimization problem with a modified gradient projection method to take advantage of the simple expression of constraints expressed in Eqs. B-8 and B-9. At each iteration of the optimization process, the search direction is obtained by projecting the gradient of the objective function on the null space of the gradients of the binding constraints (see Ref. 3 for details).

SI Metric Conversion Factors

bbl × 1.589 873	E−01	= m^3
cp × 1.0*	E−03	= Pa·s
ft × 3.048*	E−01	= m
ft^2 × 9.290 304*	E−02	= m^2
psi × 6.894 757	E+00	= kPa

*Conversion factors are exact.

SPEJ

Xian-Huan Wen currently is a lead research engineer in the geostatistics team of Chevron Petroleum Technology Co. at La Habre, California, where he works on integration of dynamic multiphase production data in geostatistical reservoir modeling. e-mail: xwen@chevron.com. He previously was a research associate in the Dept. of Petroleum Engineering at Stanford U. where his work involved geostatistical reservoir characterization, upscaling with flexible gridding, and contaminant transport modeling. Wen holds an MS degree from China U. of Geosciences and PhD degrees from Royal Inst. of Technology, Sweden, and Polytechnic U. of Valencia, Spain. **Clayton V. Deutsch** is an associate professor in the School of Mining and Petroleum Engineering, Dept. of Civil and Environmental Engineering, U. of Alberta, Edmonton, Alberta, Canada. Previously, he was an associate professor (research) in the Dept. of Petroleum Engineering at Stanford U. and worked at Exxon Production Research Center in Houston and Placer Dome, Vancouver, British Columbia. His research interests include development of geostatistical methods for data integration, construction of numerical models in the presence of sparse

data, historical production data, and complex geological architectures. Deutsch holds a BS degree in mining engineering from the U. of Alberta, and MS and PhD degrees in applied earth sciences from Stanford U. He is a member of the Editorial Review Committee and a Short Course Instructor. **A.S. (Stan) Cullick** is a scientist in Mobil's Upstream Strategic Research Center in Dallas. His current work concentrates on development of new technologies for reservoir modeling and optimization of production planning and development. His previous work involved geostatistics, upscaling, and reservoir modeling in the Reservoir Characterization Group and enhanced oil recovery, phase behavior, and special core analysis in the Improved Recovery Group. He served on the 1995–96 Forum Series in Europe Steering Committee.